AGU PUBLICATIONS

Geophysical Research Letters

RESEARCH LETTER
10.1002/2014GL060345

Key Points:
- We identify an ageostrophic instability that converges momentum toward equator
- This instability is a necessary process for the development of superrotation
- This instability is mainly controlled by Rossby and Froude numbers

Correspondence to:
P. Wang,
pengwang@epss.ucla.edu

Citation:
Wang, P., and J. L. Mitchell (2014), Planetary ageostrophic instability leads to superrotation, *Geophys. Res. Lett.*, *41*, doi:10.1002/2014GL060345.

Received 25 APR 2014
Accepted 27 MAY 2014
Accepted article online 6 JUN 2014

Planetary ageostrophic instability leads to superrotation

Peng Wang[1,2] and Jonathan L. Mitchell[1,2]

[1]Department of Earth, Planetary, and Space Sciences, University of California, Los Angeles, California, USA, [2]Department of Atmospheric and Oceanic Sciences, University of California, Los Angeles, California, USA

Abstract We demonstrate the existence of a global-scale, linear instability in the atmospheres of slowly rotating and/or small planets that spontaneously emerges and produces momentum convergence at the equator, thus supporting the development of planetary superrotation. We identify the instability as being barotropic, ageostrophic in nature, coupling an equatorial Kelvin wave with midlatitude or high-latitude Rossby waves. This coupling requires a frequency matching of the Doppler-shifted wave components and moderate spatial overlap between them, which are determined by two nondimensional parameters, the Rossby and Froude numbers. By diagnosing these parameters, we find that this instability is an essential and necessary process to obtain superrotation in dry atmospheric, general circulation models with axisymmetric forcing. The Rossby and Froude numbers for Solar System bodies are consistent with the presence or absence of superrotation, which suggests that they provide useful diagnostics for predicting the emergence of superrotation in the atmospheres of terrestrial planets.

1. Introduction

Planetary superrotation commonly refers to atmospheric circulations with persistent zonal mean westerly winds over the equator. There is a well-developed literature on the mechanism of generating and maintaining planetary superrotation. *Gierasch* [1975] suggests some required eddy process to maintain the momentum surplus at the equator against the poleward momentum transport by the large-scale meridional circulation, without identifying the underlying eddy activity. Two main categories of mechanisms have been put forward to characterize the source of this eddy activity. The first category involves the eddy momentum fluxes generated by shear instabilities of the zonal mean winds in atmospheric models with purely axisymmetric forcing, i.e., nonaxisymmetric eddies are not directly forced. For instance, *Williams* [2003, 2006] demonstrates that by moving the jet streams closer to equator, eddy momentum fluxes from the barotropic instability on the equatorward flank of the jets lead to superrotation in a dry idealized general circulation model (GCM). Most planet-specific GCMs of Venus and Titan attribute the development of superrotation to this type of spontaneously emerging barotropic instability of the midlatitude jets [e.g., *Lee et al.*, 2007; *Newman et al.*, 2011; *Lebonnois et al.*, 2012]. Without identifying a wave excitation mechanism, *Imamura et al.* [2004] and *Imamura* [2006] examine several types of equatorial waves (which refer to a set of normal-mode solutions to the linearized, β-plane shallow water equations [*Matsuno*, 1966]) in a GCM with Venus-like zonal mean winds and find that a couple of them produce equatorial momentum convergence. *Fruman et al.* [2009] find that artificially initialized equatorial mixed Rossby-gravity waves can become unstable and yield an equatorward momentum flux. *Iga and Matsuda* [2005] also demonstrate that in a uniform-depth, shallow water model with Venus-like zonal mean zonal winds, an unstable Rossby-Kelvin mode emerges with an equatorward eddy momentum flux.

The second category of mechanisms involves directly generating eddy activity through nonaxisymmetric forcing. Different types of longitudinally varying forcing have been tested in nonlinear simulations. Several examples of time varying forcing that successfully produce superrotation include the following: random, small-scale forcing in the shallow water system [*Scott and Polvani*, 2008]; stationary heating on the equator in a two-layer, primitive-equation model [*Saravanan*, 1993; *Shell and Held*, 2004]; radiative heating in GCMs of tidally locked exoplanets [*Showman and Polvani*, 2010, 2011]; equatorial convection in GCMs of gas giants [*Schneider and Liu*, 2009; *Lian and Showman*, 2010; *Liu and Schneider*, 2011]; and zonally propagating tropical heating in a dry, terrestrial GCM [*Arnold et al.*, 2012].

The Rossby number, usually defined as $Ro = U_0/fL$, represents the relative importance between the advection and rotation dynamics, where U_0 and L are the characteristic velocity and length scales of the

phenomena of interest, and $f = 2\Omega \sin\varphi$ is the Coriolis parameter for a planet with rotation rate Ω. More specifically, $Ro \ll 1$ indicates geostrophic or gradient-wind balanced dynamics, while $Ro \sim 1$ indicates more complicated dynamics that may, for instance, involve fast, unbalanced dynamics (i.e., gravity waves) coupled with slow, balanced dynamics (e.g., Rossby waves). On Earth, both regimes coexist with $Ro \sim 1$ very near the equator and $Ro \ll 1$ at middle and high latitudes (as it is on Jupiter and Saturn). On Titan and Venus, the large-*Ro* regime dominates the entire globe. Equatorial superrotation is therefore intrinsically a large-*Ro* phenomenon, suggesting its mechanism may involve the coupling of fast and slow dynamics.

Motivated by this, *Mitchell and Vallis* [2010] demonstrate that by increasing a single parameter, the thermal Rossby number $Ro_T = RT_0\Delta_H/(2\Omega a)^2$ (where R is the gas constant, T_0 is the global average temperature, Δ_H is the equator-to-pole temperature gradient, and a is the planetary radius); global atmospheric simulations with axisymmetric forcing pass from an Earth-like atmosphere for $Ro_T \ll 1$ to superrotating one like Titan and Venus for large $Ro_T > 1$. It is demonstrated in both *Mitchell and Vallis* [2010] and *Potter et al.* [2014] that the generation of superrotation involves a global mode that appears to couple Rossby and Kelvin waves. In this paper, our two primary motivations are (1) to identify the instability that generates spontaneous (i.e., unforced) superrotation in global simulations and (2) to develop a simple diagnostic for classifying planetary circulation regimes, in particular the emergence of superrotation. In section 2, we describe our model of linear instability analysis in planetary atmospheres. In section 3, we identify the nature and parameter regime of this instability. In section 4, our diagnostic parameters are evaluated for the idealized GCM simulations from *Mitchell et al.* [2014] and several terrestrial bodies in Solar System, and compared with the theory from the linear analysis in section 3. We conclude with a discussion in section 5.

2. Linear Instability Analysis

In order to explore the instability that may converge zonal momentum toward equator, we start from a linear instability analysis of idealized shear flows with various *Ro* based on the wind profiles from the numerical simulations in *Mitchell and Vallis* [2010]. The Eliassen-Palm flux (the divergence of which represents the acceleration of the zonal mean winds [*Andrews and McIntyre*, 1976]) from the Titan-like simulation in *Mitchell and Vallis*, [2010, Figure 7, middle plot] has shown that the acceleration of equatorial zonal winds is mainly caused by the horizontal momentum convergence in the spin-up stage. This indicates that the instability that induces the eddy momentum transport is mostly barotropic, i.e., the instability occurs primarily due to the meridional shear rather than the vertical shear. Therefore, we examine a series of barotropic, meridional shear flows $\overline{U}(\varphi)$. As in the simulations, the idealized meridional shear profiles are angular momentum conserving near the equator and their magnitude vanishes close to the poles. The analytical form of $\overline{U}(\varphi)$ is

$$\overline{U}(\varphi) = \begin{cases} \frac{\Omega a \sin^2\varphi}{\cos\varphi} & |\varphi| \le \varphi_0 \\ \frac{\Omega a \sin^2\varphi}{\cos\varphi} e^{-\alpha(|\varphi|-\varphi_0)^2} & |\varphi| > \varphi_0 \end{cases}, \tag{1}$$

where φ is the latitude, Ω and a are the planetary angular velocity and radius, respectively, and α is a factor that controls the decay of the profile toward the poles, whose value depends on φ_0. Here we introduce an important varying parameter φ_0 representing the latitude beyond which the shear profile is no longer angular momentum conserving (i.e., the winds are modified by a Gaussian roll-off beyond φ_0), which determines both the latitudinal location and the magnitude of the maximum winds.

We examine the linear instabilities of the above $\overline{U}(\varphi)$ profiles in linearized, hydrostatic, Boussinesq equations (considering small density variation compared to the reference state, 2.4.2 in *Vallis* [2006]) in spherical coordinates. In order to apply our linear theory to a large range of general cases, we study the problem in a set of nondimensional equations. The variables are scaled as follows:

$$(x, y, z, t) \sim (a, a, H, 1/2\Omega), \quad (u, v, w) \sim (U_0, U_0, U_0 H/a), \quad p \sim 2\Omega U_0 \rho_0 a, \quad (\theta, T) \sim 2\Omega U_0 a/R,$$

where u and v (w) are horizontal (vertical) velocities, p is pressure, θ and T are potential temperature and temperature, respectively, ρ_0 is the average atmospheric density, and R is the gas constant. Here the

characteristic velocity scale U_0 is defined by the maximum of the meridional shear $\overline{U}(\varphi)$. With these scalings, the nondimensional, linearized equations are

$$\begin{aligned}
\frac{\partial u'}{\partial t} + Ro\left(\frac{\overline{U}}{\cos\varphi}\frac{\partial u'}{\partial \lambda} + v'\frac{\partial \overline{U}}{\partial \varphi}\right) - (\sin\varphi + Ro\overline{U}\tan\varphi)v' + \frac{1}{\cos\varphi}\frac{\partial p'}{\partial \lambda} &= 0\\
\frac{\partial v'}{\partial t} + Ro\frac{\overline{U}}{\cos\varphi}\frac{\partial v'}{\partial \lambda} + (\sin\varphi + Ro\overline{U}\tan\varphi)u' + \frac{\partial p'}{\partial \varphi} &= 0\\
\frac{\partial p'}{\partial z} - T' &= 0\\
\frac{1}{\cos\varphi}\frac{\partial u'}{\partial \lambda} + \frac{1}{\cos\varphi}\frac{\partial}{\partial \varphi}(v'\cos\varphi) + \frac{\partial w'}{\partial z} &= 0\\
\frac{\partial T'}{\partial t} + Ro\frac{\overline{U}}{\cos\varphi}\frac{\partial T'}{\partial \lambda} + Buw' &= 0\,,
\end{aligned} \tag{2}$$

where λ is the longitude. There are two nondimensional, control parameters in (2), the Rossby number and the Burger number:

$$Ro = \frac{U_0}{2\Omega a}, \quad Bu = \left(\frac{NH}{2\Omega a}\right)^2, \tag{3}$$

where N is the Brunt-Väisälä frequency, denoting the background stratification. *Bu* represents the importance of the stratification compared to the rotation. By varying φ_0, we obtain a series of meridional shear profiles with different U_0 and *Ro*. We can independently vary *Bu* to control the relative importance of the background stratification.

Assuming the nondimensional perturbation variables are normal-mode solutions,

$$\{u', v', w', p', T'\} \sim \{\hat{u}, \hat{v}, \hat{w}, \hat{p}, \hat{T}\}(\varphi)e^{ik\lambda+\tilde{\sigma}t}\sin(mz)\,,$$

where k and m are the zonal and vertical wave numbers of the perturbations, respectively, the equation (2) becomes an eigenvalue problem in y that can be solved numerically, with $\sigma = \text{Real}(\tilde{\sigma})$ the growth rate and $\omega = -\text{Imag}(\tilde{\sigma})$ the frequency of the mode. The meridional boundary conditions are set as $v' = \partial u'/\partial y = \partial w'/\partial y = \partial p'/\partial y = \partial T'/\partial y = 0$ at the poles. The vertical boundary conditions are set as $w' = \partial u'/\partial z = \partial v'/\partial z = \partial p'/\partial z = \partial T'/\partial z = 0$ at the top and bottom boundaries, therefore the values of m can only be integer multiples of π.

By conducting the linear instability analysis on the global meridional shear flow $\overline{U}(\varphi)$ with varying φ_0 and *Bu*, we aim to address the following questions: (1) What is the instability that converges the zonal momentum toward equator? (2) What is the parameter regime for the occurrence of the instability?

In the Titan-like simulation of *Mitchell and Vallis* [2010] (Figures 9 and 14), a global mode with zonal wave number around 1 is responsible for equatorial momentum convergence leading to superrotation, so we let $k = 1$ in our linear analysis. Due to the ambiguity of the vertical scale of the mean flow $\overline{U}(\varphi)$ (i.e., there is no clear definition for the vertical scale of $\overline{U}(\varphi)$), H and m are both determined by the vertical scale of the perturbations and hence are not independent. Since H can be varied with *Bu*, we choose to fix $m = \pi$ (the first baroclinic mode) in the eigenvalue problem. In the next section, we will discuss the linear solutions and address the above questions.

3. Barotropic, Rossby-Kelvin Instability

By solving the normal-mode solutions to (2), we find two types of instability in the examined $\overline{U}(\varphi)$. The first one is the classic barotropic instability that relates to the inflection points (where potential vorticity gradient changes sign [*Rayleigh*, 1880]) in the meridional shear, which does not lead to an equatorward zonal momentum transport. The other one is a type of barotropic, ageostrophic instability that does not exist in the quasi-geostrophic regime; we call it Rossby-Kelvin (RK) instability. The eddy momentum flux of the RK instability converges at the equator; and therefore, this instability acts as a potential mechanism for equatorial superrotation.

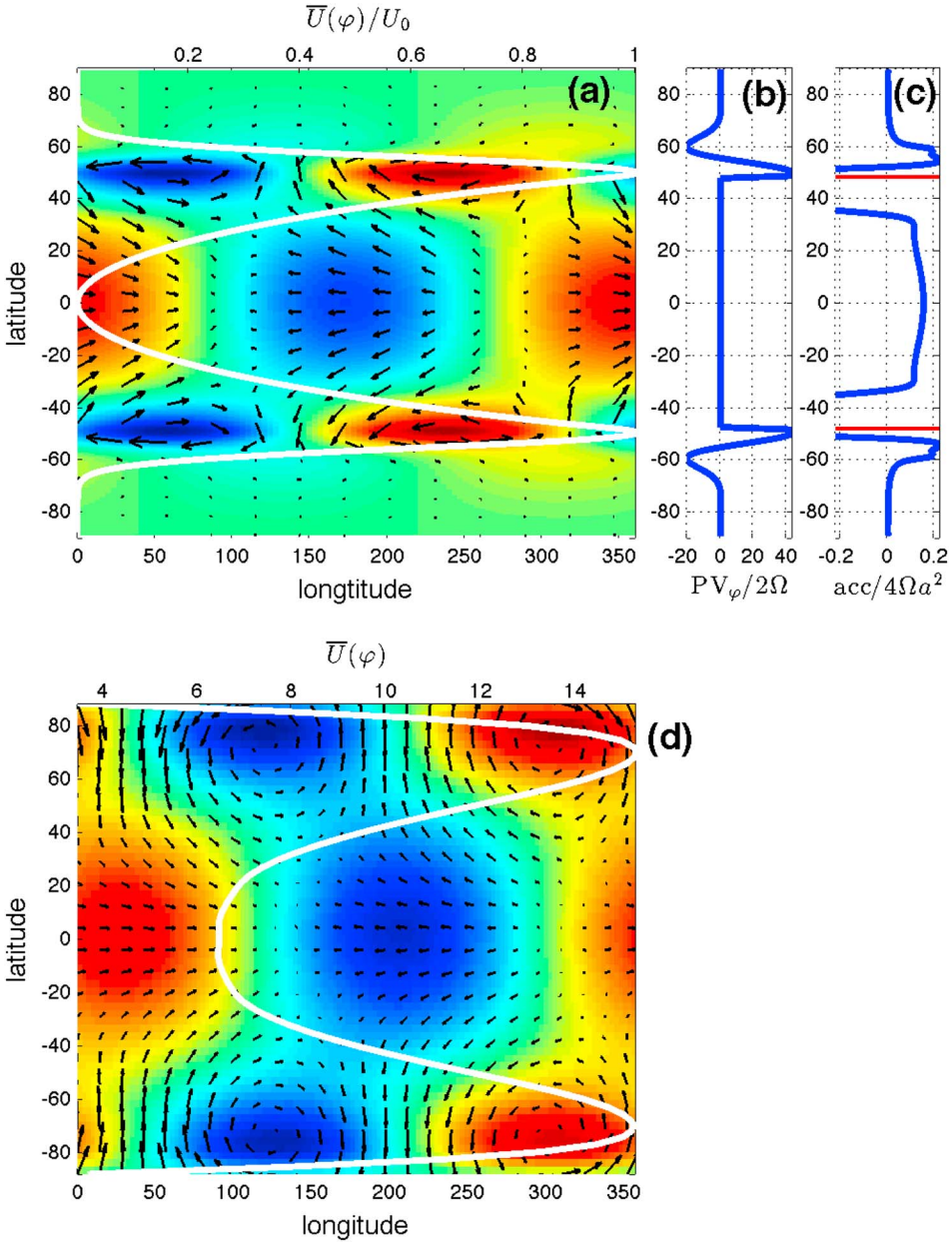

Figure 1. (a) The longitude-latitude pattern for pressure perturbation (red represents positive, blue represents negative) and wind anomalies (vectors) of an unstable Rossby-Kelvin mode from our linear analysis with $Bu = 0.8$ and $\varphi = 50°$ ($Ro = 0.43$ and $Fr = 1.12$, φ_0 denoted by red line in Figure 1c), and the associated mean background meridional shear $\overline{U}(\varphi)$ (white line, scaled by U_0). (b) The potential vorticity gradient PV_φ of the mean shear used in our linear analysis (scaled by 2Ω). (c) The zonal momentum acceleration of the linear, unstable mode (Figure 1a) as a function of latitude (scaled by $4a\Omega^2$). (d) The 700 hPa geopotential height perturbation (color) and wind anomalies (vectors) of the mode accelerating the equatorial zonal winds, and vertical and zonal mean zonal wind (white line) (both) from the Titan-like simulation of *Mitchell and Vallis* [2010].

The perturbation pattern of an unstable RK mode and the mean meridional shear (scaled by U_0) is shown in Figure 1a. Figure 1b shows the potential vorticity (PV) gradient of $\overline{U}(\varphi)$ (scaled by 2Ω) for the mean shear,

$$\mathrm{PV}_\varphi = \frac{\partial}{\partial\varphi}\left[2\Omega\sin\varphi - \frac{1}{a\cos\varphi}\frac{\partial}{\partial\varphi}(\overline{U}\cos\varphi)\right]. \quad (4)$$

The zonal momentum acceleration of the mean winds by the unstable perturbations (scaled by $4a\Omega^2$) is shown in Figure 1c. It is calculated as

$$\text{acceleration} = \frac{1}{a^2 \cos^2 \varphi} \frac{\partial}{\partial \varphi} \left(-a \cos^2 \varphi \overline{u'v'} \right) . \tag{5}$$

The RK mode is a global mode that couples the equatorial Kelvin wave and the midlatitude or high-latitude Rossby waves. In the coupled mode, the Rossby waves reside in the jet region, where the PV gradient is nonzero; and the Kelvin wave is trapped near the equator, where PV gradient is zero. The perturbations of the RK instability prominently accelerate the zonal mean winds near the equator, i.e., in the Kelvin wave component region. The unstable RK mode pattern in our linear analysis (Figure 1a) is very similar to the mode that accelerates the zonal winds at the equator in the Titan-like simulation of *Mitchell and Vallis* [2010] (Figure 1d). The mode shown in Figure 1d is filtered for zonal wave number 1 and frequency 0.6 day^{-1}, and the mean wind and temperature profiles have $Ro = 0.43$ and $Bu = 0.8$. For this pair of Ro and Bu, the unstable RK mode in our linear analysis has a frequency around 0.5 day^{-1}, which is consistent with the simulation. The consistency in both the pattern and the frequency confirms the role of RK instability in leading to equatorial superrotation. Note that the idealized midlatitude or high-latitude jets in the linear analysis are much sharper than the ones in the numerical simulation; and therefore, the Rossby wave components in our theoretical experiments appear in a much narrower latitudinal band than in the simulations.

By varying φ_0 and Bu, we find this RK instability in a variety of parameter regimes, with similar perturbation patterns to Figure 1a, but different meridional scales of the Kelvin wave component and locations of the Rossby wave components. The growth rate of this instability as a function of Bu and φ_0, and the mode pattern for several particular Bu and φ_0 pairs is shown in Figure 2. With the locations of the midlatitude or high-latitude jets fixed, the RK instability only occurs within a certain range of Bu. For instance, the modes in Figures 2b and 2d both have $\varphi_0 = 60°$ but with different Bu. Both modes have Rossby waves residing at ~60°, but the strength of the instability (growth rate) is different. The meridional scale of the Kelvin wave component is mainly determined by the equatorial deformation radius. In β-plane, linearized Boussinesq equations with zero mean winds, a Kelvin wave is trapped along the equator within an equatorial deformation radius, $\sqrt{2N/(\beta m)}$, where m is the vertical wave number of the wave. By comparing with (3), we see the trapping of the equatorial Kelvin wave is controlled by Bu. When the deformation radius is small and the midlatitude or high-latitude jets are far from equator, the coupling between the Rossby waves and Kelvin wave is weak and hence the instability is weak. By comparing the modes in Figures 2c and 2d, which have the same Bu, we find that when the jets are shifted closer to equator, the coupling becomes stronger.

The equatorward eddy momentum flux makes the RK instability an essential and necessary process leading to planetary superrotation in global simulations with only axisymmetric forcing. The global simulations are characterized by several important nondimensional parameters such as the Rossby, Froude, Burger, Ekman, Prantl numbers, etc. For the purpose of classifying planetary circulation regimes, we now investigate the parameter regimes for the occurrence of the RK instability. The physical interpretation of this instability can be described as a coupling of equatorial Kelvin wave and midlatitude or high-latitude Rossby waves. The condition for their resonant coupling is that the two types of waves have the same frequency. As a measure of this effect, we define the Froude number as

$$Fr = \frac{U_0/\cos\varphi_{\max}}{U_{\text{eq}} + NH/m} = \frac{Ro/\cos\varphi_{\max}}{U_{\text{eq}}/(2\Omega a) + \sqrt{Bu}/m} , \tag{6}$$

where U_{eq} is the value of the equatorial wind (zero for $\overline{U}(\varphi)$ in (1)) and $\varphi_{\max}$ is the latitude for the maximum zonal winds. Fr is simply the ratio of the Doppler-shifted frequency of the midlatitude or high-latitude Rossby waves to that of the equatorial Kelvin wave. According to the physical interpretation of the RK instability, we expect the resonant coupling to occur in a certain range of Fr. For an unstable, coupled RK mode, the frequencies of the two types of waves coincide exactly, and their ratio is unity. However, the estimated Fr in (6) is not unity due to the ambiguity of the frequency of a Rossby wave in a smoothly varying meridional shear. As an approximation, we neglect the small, westward intrinsic component in the Rossby wave frequency and use the maximum wind to represent the Doppler-shift by the jet, so the instability can occur for a range of Fr.

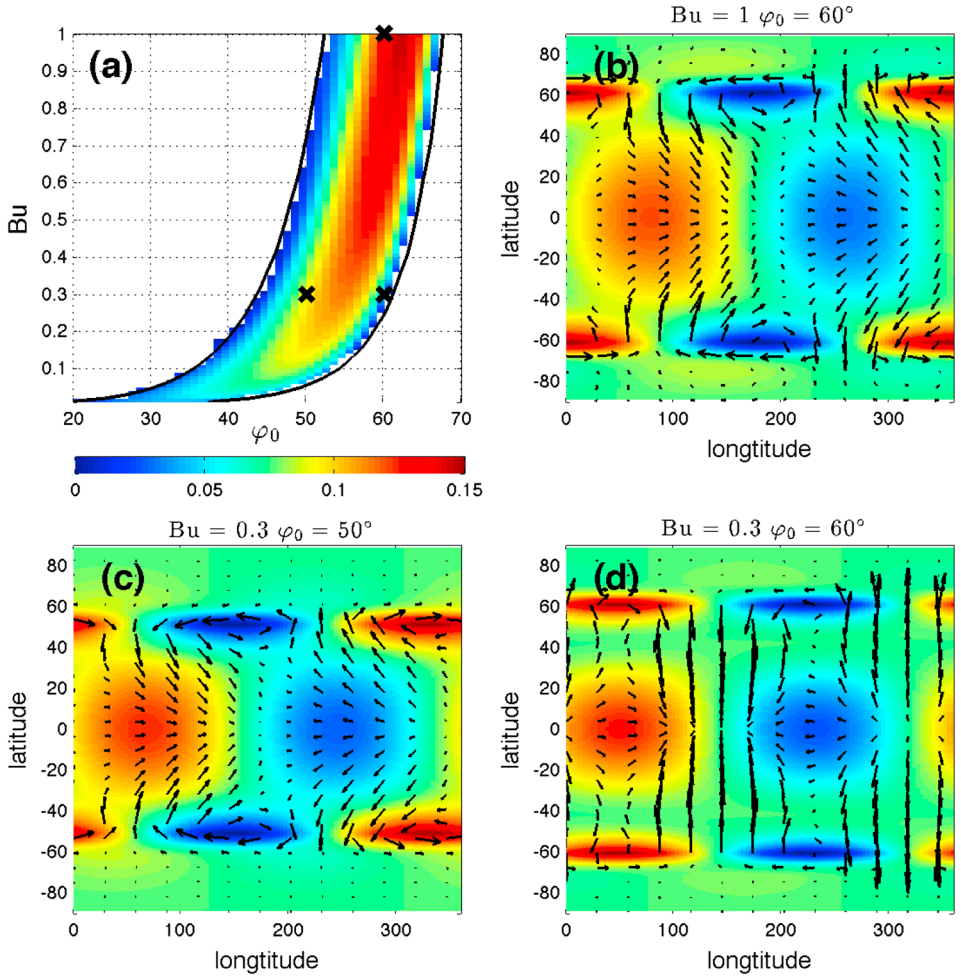

Figure 2. (a) The growth rate σ (scaled by 2Ω) of the linear Rossby-Kelvin instability as a function of *Bu* and φ_0. The longitude-latitude pattern (color: pressure perturbation, vector: wind anomalies) of the RK mode for the three (*Bu*, φ_0) pairs denoted by the crosses in Figure 2a. (b) $Bu = 1$, $\varphi_0 = 60°$, and $\sigma/2\Omega = 0.18$; (c) $Bu = 0.3$, $\varphi_0 = 50°$, and $\sigma/2\Omega = 0.20$; (d) $Bu = 0.3$, $\varphi_0 = 60°$, and $\sigma/2\Omega = 0.02$. The two black lines that enclose nonzero growth rate in Figure 2a are contours for *Fr* about 1 and 3, respectively.

Figure 3 shows the growth rate of the RK instability (scaled by 2Ω) and the zonal momentum acceleration at the equator by the unstable perturbations (scaled by $4a\Omega^2$) as a function of (*Ro*, *Fr*). The RK mode is almost stable for small *Ro* planets (Earth-like), and its strength increases as *Ro* increases. For each *Ro*, the instability only occurs within a band of *Fr* roughly between 1 and 3; as *Ro* increases, the band becomes narrower. The two black lines that roughly enclose the positive growth rate on a (φ_0, *Bu*) space in Figure 2a are for constant values of *Fr* of about 1 and 3, which demonstrates the utility of *Fr* in characterizing the resonant coupling of the RK mode. The zonal momentum acceleration at the equator (Figure 3b) occurs over the same range of positive growth rate: A stronger RK instability has a more efficient momentum transport toward equator, and hence possibly leads to more robust superrotation.

4. Simulation Diagnostics for Nondimensional Parameters

In section 3, we identified the RK instability as a possible mechanism to accelerate zonal winds at the equator and examined the parameter regime for its occurrence. Furthermore, we confirmed that the pattern and frequency of the RK mode are consistent with those of the mode that accelerates the equatorial winds in the Titan-like simulation of *Mitchell and Vallis* [2010]. In order to investigate whether the above theory is generally predictive of the circulation regimes supporting superrotation, we diagnose the characteristic, nondimensional parameters from idealized simulations as well as planetary wind and static stability measurements, and compare them with the predicted parameter range for the RK instability. In the linear

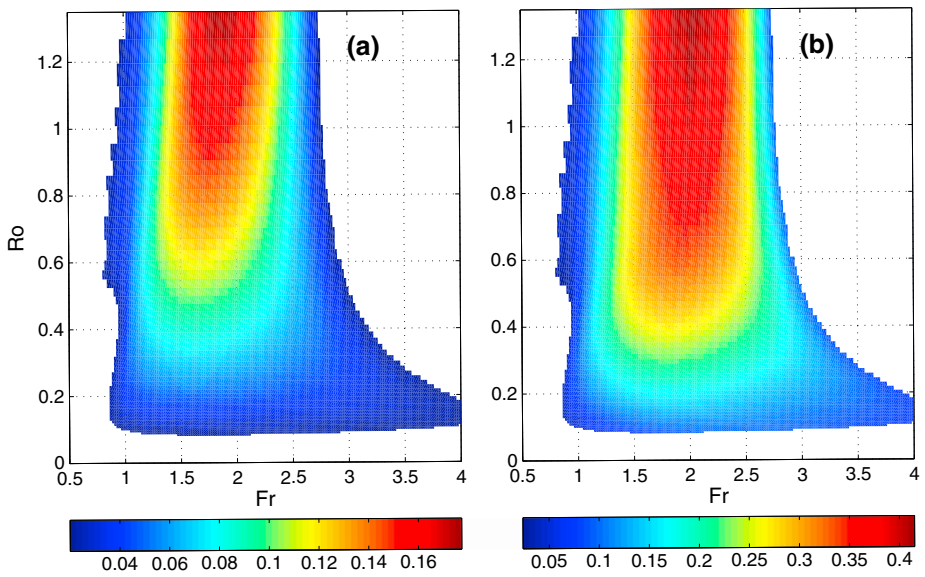

Figure 3. The (a) growth rate σ and (b) zonal momentum acceleration at equator of the Rossby-Kelvin instability on a (*Fr*, *Ro*) space. The growth rate σ is scaled by the rotation rate 2Ω, and the zonal momentum acceleration is scaled by $4a\Omega^2$.

instability analysis in sections 2 and 3, the mean wind at the equator, U_{eq}, is zero; while in realistic global circulations, the equatorial wind is commonly nonzero and sometimes comparable to the phase speed of the Kelvin wave. We diagnose U_0, φ_{max}, and U_{eq} based on the vertical and zonal mean zonal winds, and calculate N from the globally averaged value of stratification, H as the scale height and $m = \pi$ as the vertical wave number.

The diagnosed *Ro* and *Fr* from the idealized global simulations with five thermal Rossby numbers from *Mitchell et al.* [2014] and from a simulation of Titan's climate and reanalysis data for Earth and Mars are shown in Figure 4. We use National Centers for Environmental Prediction/National Center for Atmospheric Research (NCEP/NCAR) Reanalysis data set for Earth, Mars Analysis Correction Data Assimilation (MACDA, MGS/TES v1.0) data set from NERC Centres for Atmospheric Science (NCAS) British Atmospheric Data Centre for Mars [*Montabone et al.*, 2011], and a realistic global simulation data for Titan [*Mitchell et al.*, 2011; *Mitchell*, 2012]. Note that the Ro_T in *Mitchell et al.* [2014] is defined as $Ro_T = (RT_0\Delta_H)/(2\Omega a)^2$ with fixed T_0, Δ_H, Ω, and varying a, while our definition here is different: $Ro = U_0/2\Omega a$ with U_0 the maximum zonal wind. For the simulations, we plot a series of (*Fr*, *Ro*) values from the mean states averaged in time bins of 90 days over the full 1080 days starting from a state of rest. The nonsuperrotating cases ($Ro_T = 0.02$ and Ro_T=0.08) have small *Ro*, and the RK instability is too weak to accelerate the equatorial winds. As Ro_T increases, the circulation starts to fall in the right (*Fr*, *Ro*) regime for the RK instability, and equatorial superrotation develops. The figure clearly shows a positive correlation between the magnitude of the equatorial winds (a superrotation index) and the growth rate of the RK instability, which confirms that the RK instability is an essential process leading to superrotation in global simulations with axisymmetric forcing. In the intermediate Ro_T simulations (1.3 and 3.1), there is weak superrotation and the instability occurs intermittently throughout the time evolution. However, in the simulation with $Ro_T = 10.5$, this instability strongly accelerates equatorial winds in the spin-up stage, while the instability is very weak in the steady state (U_{eq} is large so *Fr* becomes small), indicating some other processes play an important role in the maintenance of superrotation in this case. The disappearance of the RK mode after the circulation reaches steady state is also shown in Figure 13 of *Mitchell and Vallis* [2010].

The diagnosed *Ro* and *Fr* from reanalysis data for Earth and Mars, and the 3-D simulation for Titan are also shown in Figure 4. The parameters are calculated from the annual-mean wind and temperature profiles of the steady state data. Earth and Mars have a global circulation without superrotation, and their bulk (*Fr*, *Ro*) fall in the regime where the RK instability does not occur. The (*Fr*, *Ro*) for Titan falls in the regime close to that for the steady state circulation of the $Ro_T = 10.5$ simulation, where RK instability does not occur either. The Titan model lies at the end of the progression shown for the $Ro_T = 10.5$ case, suggesting it spins up by

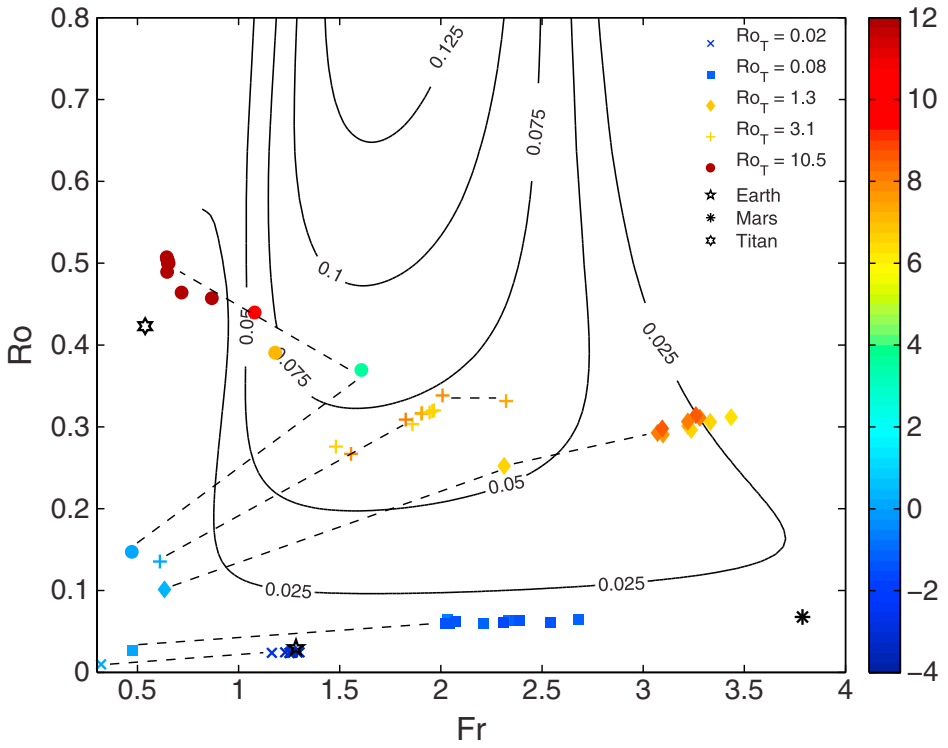

Figure 4. A scatterplot of diagnosed *Ro* and *Fr* from numerical simulations in *Mitchell et al.* [2014] (color symbols), the reanalysis data for Earth and Mars, and the realistic 3-D simulations for Titan (black symbols) overplotted on the theoretical growth rate values (black contours, scaled by 2Ω) of the Rossby-Kelvin instability as in Figure 3a. The *Ro* and *Fr* calculated from numerical simulations are based on the mean states averaged over every 90 days of 1080 day integrations (dashed lines demonstrate progression in simulated time), and those from realistic planetary data with seasons (black symbols) are based on the annual-mean winds and temperature profiles and the characteristic physical parameters of the planets. For the diagnostics from idealized simulations (color symbols), the colors of the markers represent the magnitudes of the zonal winds at the equator, and the marker types represent different Ro_T cases as labeled.

the same mechanism. As discussed above, the RK instability is responsible for the spin-up of this strongly superrotating circulation but not necessarily for the maintenance of it.

5. Conclusion

We have demonstrated the existence of a global-scale, linear instability for moderate-*Ro* (0.1–1) planetary atmospheres that spontaneously emerges and produces momentum convergence at the equator, thus supporting the development of superrotation. We identify the instability as being barotropic, ageostrophic in nature (a meridional shear instability) that couples the equatorial Kelvin wave with mid-latitude or high-latitude Rossby waves (Figure 1). This coupling requires (1) a frequency matching of the Doppler-shifted wave components and (2) moderate spatial overlap between them. These two conditions are determined by the bulk Froude number, *Fr* (Figure 3), and the combination of the jet location ϕ_0 and the Burger number *Bu* (Figure 2), respectively. Because *Ro*, *Bu*, and *Fr* are not independent, the primary control parameters for this instability are just *Ro* and *Fr*.

By diagnosing these nondimensional parameters in GCM simulations, we demonstrate that the Rossby-Kelvin instability is an essential and necessary process to obtain superrotation in dry atmospheric, global simulations with axisymmetric forcing (Figure 4). The strength of the equatorial superrotation is positively correlated with the strength of the Rossby-Kelvin instability. However, this instability is not sufficient for the occurrence of superrotation. As shown in *Dias Pinto and Mitchell* [2014], the strength of Hadley cell also has significant influence on the equatorial superrotation. Though the rising component transports momentum upward at the equator, the poleward component of the Hadley cell removes eastward zonal momentum from the equator, which acts against the eddy momentum transport by the Rossby-Kelvin instability. It is shown that if the Hadley cell is strong enough in large-*Ro* simulations, the superrotation dis-

appears. Baroclinic instability, with eddy momentum flux toward midlatitude, also plays an opposing role to the Rossby-Kelvin instability. *Mitchell et al.* [2014] have shown that superrotation only occurs in idealized simulations when the baroclinic super criticality is not large.

The values of *Ro* and *Fr* for Solar System bodies (Earth, Mars, and Titan) are also estimated in our work, and their values are consistent with the presence of superrotation on Titan and the absence of it on Earth or Mars (Figure 4). This result suggests that the *Ro* and *Fr* provide useful diagnostics for predicting the emergence of superrotation in the atmospheres of terrestrial planets.

Acknowledgments

This work was supported by NASA grant NNX12AI71G to the University of California, Los Angeles. The data for Earth are available at NOAA Earth System Research Laboratory Physical Sciences Division. Data set: NCEP/NCAR Reanalysis 1. The data for Mars is available at NCAS British Atmospheric Data Centre. Data set: Mars Analysis Correction Data Assimilation (MACDA): MGS/TES v1.0.

The Editor thanks two anonymous reviewers for their assistance in evaluating this paper.

References

Andrews, D. G., and M. E. McIntyre (1976), Planetary waves in horizontal and vertical shear: The generalized eliassen-palm relation and the mean zonal acceleration., *J. Atmos. Sci.*, *33*(11), 2031–2048.

Arnold, N. P., E. Tziperman, and B. Farrell (2012), Abrupt transition to strong superrotation driven by equatorial wave resonance in an idealized GCM, *J. Atmos. Sci.*, *69*, 626–640.

Dias Pinto, J., and J. Mitchell (2014), Atmospheric superrotation in an idealized gcm: Parameter dependence of the eddy response, *Icarus*, *238*, 93–109, doi:10.1016/j.icarus.2014.04.036.

Fruman, M. D., B. L. Hua, and R. Schopp (2009), Equatorial zonal jet formation through the barotropic instability of low-frequency mixed rossby-gravity waves, equilibration by inertial instability, and transition to superrotation, *J. Atmos. Sci.*, *66*, 2600–2619.

Gierasch, P. J. (1975), Meridional circulation and the maintenance of the Venus atmospheric rotation, *J. Atmos. Sci.*, *32*, 1038–1044.

Iga, S.-I., and Y. Matsuda (2005), Shear instability in a shallow water model with implications for the Venus atmosphere, *J. Atmos. Sci.*, *62*, 2514–2527.

Imamura, T. (2006), Meridional propagation of planetary-scale waves in vertical shear: Implication for the Venus atmosphere, *J. Atmos. Sci.*, *63*, 1623–1636.

Imamura, T., T. Horinouchi, and T. J. Dunkerton (2004), The lateral transport of zonal momentum due to Kelvin waves in a meridional circulation, *J. Atmos. Sci.*, *61*, 1966–1975.

Lebonnois, S., J. Burgalat, P. Rannou, and B. Charnay (2012), Titan global climate model: A new 3-dimensional version of the IPSL Titan GCM, *Icarus*, *218*(1), 707–722.

Lee, C., S. R. Lewis, and P. L. Read (2007), Superrotation in a Venus general circulation model, *J. Geophys. Res.*, *112*, E04S11, doi:10.1029/2006JE002874.

Lian, Y., and A. P. Showman (2010), Generation of equatorial jets by large-scale latent heating on the giant planets, *Icarus*, *207*, 373–393.

Liu, J., and T. Schneider (2011), Convective generation of equatorial superrotation in planetary atmospheres, *J. Atmos. Sci.*, *68*, 2742–2756.

Matsuno, T. (1966), Quasi-geostrophic motions in the equatorial area, *J. Meteorol. Soc. Japan*, *44*(1), 25–43.

Mitchell, J. L. (2012), Titan's transport-driven methane cycle, *Astrophys. J.*, *756*, L26, doi:10.1088/2041-8205/756/2/L26.

Mitchell, J. L., and G. K. Vallis (2010), The transition to superrotation in terrestrial atmospheres, *J. Geophys. Res.*, *115*, E12008, doi:10.1029/2010JE003587.

Mitchell, J. L., M. Adamkovics, R. Caballero, and E. P. Turtle (2011), Locally enhanced precipitation organized by planetary-scale waves on Titan, *Nat. Geosci.*, *4*, 589–592, doi:10.1038/ngeo1219.

Mitchell, J. L., G. K. Vallis, and S. F. Potter (2014), Effects of the seasonal cycle on superrotation in planetary atmospheres, *Astrophys. J.*, *786*, 23, doi:10.1088/0004-637X/787/1/23.

Montabone, L., S. R. Lewis, and P. L. Read (2011), Mars Analysis Correction Data Assimilation (MACDA): MGS/TES v1.0, NCAS British Atmospheric Data Centre, doi:10.5285/78114093-E2BD-4601-8AE5-3551E62AEF2B.

Newman, C. E., C. Lee, Y. Lian, M. I. Richardson, and A. D. Toigo (2011), Stratospheric superrotation in the titanWRF model, *Icarus*, *213*(2), 636–654.

Potter, S. F., G. K. Vallis, and J. Mitchell (2014), Spontaneous superrotation and the role of Kelvin waves in an idealized dry GCM, *J. Atmos. Sci.*, *71*, 596–614.

Rayleigh, L. (1880), On the stability, or instability, of certain fluid motions, *Proc. London Math. Soc.*, *11*, 57–70.

Saravanan, R. (1993), Equatorial superrotation and maintenance of the general circulation in two-level models, *J. Atmos. Sci.*, *50*(9), 1211–1227.

Schneider, T., and J. Liu (2009), Formation of jets and equatorial superrotation on Jupiter, *J. Atmos. Sci.*, *66*, 579.

Scott, R. K., and L. M. Polvani (2008), Equatorial superrotation in shallow atmospheres, *Geophys. Res. Lett.*, *35*, L24202, doi:10.1029/2008GL036060.

Shell, K. M., and I. M. Held (2004), Abrupt transition to strong superrotation in an axisymmetric model of the upper troposphere, *J. Atmos. Sci.*, *61*(23), 2928–2935.

Showman, A. P., and L. M. Polvani (2010), The Matsuno-Gill model and equatorial superrotation, *Geophys. Res. Lett.*, *37*, L18811, doi:10.1029/2010GL044343.

Showman, A. P., and L. M. Polvani (2011), Equatorial superrotation on tidally locked exoplanets, *Astrophys. J.*, *738*, 71.

Vallis, G. K. (2006), *Atmospheric and Oceanic Fluid Dynamics*, 745 pp., Cambridge Univ. Press, Cambridge, U. K.

Williams, G. P. (2003), Barotropic instability and equatorial superrotation, *J. Atmos. Sci.*, *60*, 2136–2152.

Williams, G. P. (2006), Equatorial superrotation and barotropic instability: Static stability variants., *J. Atmos. Sci.*, *63*, 1548–1557.